PHYSICAL REVIEW D **95,** 116001 (2017)

Diphoton signal of the light Higgs boson in natural NMSSM

Junjie Cao,[1,2,*] Xiaofei Guo,[1] Yangle He,[1] Peiwen Wu,[3,†] and Yang Zhang[4]

[1]*College of Physics and Materials Science, Henan Normal University, Xinxiang 453007, China*
[2]*Department of Applied Physics, Xi'an Jiaotong University, Xi'an 710049, China*
[3]*School of Physics, KIAS, 85 Hoegiro, Seoul 02455, Republic of Korea*
[4]*State Key Laboratory of Theoretical Physics, Institute of Theoretical Physics, Academia Sinica, Beijing 100190, China*

(Received 7 February 2017; published 6 June 2017)

The natural Next-to-Minimal Supersymmetric Standard Model (nNMSSM) is featured by predicting one *CP*-even Higgs boson satisfying $m_{h_1} \lesssim 120$ GeV and Higgsinos lighter than about 300 GeV, and consequently, the cross section for dark matter (DM)-nucleon scattering in this scenario is usually quite large. We study the diphoton signal of the light Higgs boson in nNMSSM by considering the tight constraints from the latest LUX and PandaX-II experiments, and we conclude that the optimal value of the signal rate at 8 TeV LHC is greatly reduced in comparison with earlier predictions. For example, previous studies indicated that the rate may exceed 120 fb for $m_{h_1} \simeq 80$ GeV, while it is at most 25 fb if the lightest neutralino in the scenario is fully responsible for the measured DM relic density. We also investigate the case of $m_{h_1} \simeq 98$ GeV, which is hinted by the excesses of the large electron proton collider analysis on $Z\bar{b}b$ signal and the compact muon solenoid analysis on the diphoton signal. We conclude that nNMSSM can simultaneously explain the excesses at the 1σ level without violating any known constraints.

DOI: 10.1103/PhysRevD.95.116001

I. INTRODUCTION

The hierarchy problem of the Standard Model (SM) usually implies a more complex structure in the Higgs sector to explain the electroweak symmetry breaking. In the present context of continuing efforts paid to search for new particles at the upgraded LHC, it is one of the priorities to look for extra Higgs bosons. Since, experimentally, a photon is a very clean object and can be reconstructed with a very high precision. The diphoton signal of the bosons has been considered the golden channel in the search, especially when the bosons are moderately light, and one remarkable achievement in this direction is the great discovery of a 125 GeV Higgs boson in 2012 [1,2]. On the theoretical side, supersymmetric theory provides an elegant way to stabilize the electroweak scale, and it is regarded as one of the most promising candidates of new physics. However, in order to accommodate a Higgs boson with its mass around 125 GeV in the Minimal Supersymmetric Standard Model (MSSM), the contribution to the mass from higher order correction is required to be very close to its tree-level value, which seems rather unnatural [3]. As a result, nonminimal supersymmetric theories have drawn a lot attention in recent years. In this work we concentrate on the Next-to-Minimal Supersymmetric Standard Model (NMSSM) [4], which is the simplest extension of the MSSM with one singlet Higgs field. To be more specific, we study the diphoton signal of the lightest *CP*-even Higgs boson in the most attractive scenario of the NMSSM, which is dubbed as a natural NMSSM (nNMSSM) [5].

The essential feature of the nNMSSM is that among the three *CP*-even Higgs bosons predicted by the NMSSM, the next to lightest one corresponds to the 125 GeV Higgs, which is usually called the SM-like Higgs boson, and in order to achieve this, the Higgsino mass parameter μ is preferred to be lighter than about 300 GeV [5,6]. In this scenario, the Higgs mass can be lifted by both a singlet-doublet-doublet Higgs coupling and a singlet-doublet Higgs mixing, and consequently, its value can be easily enhanced to 125 GeV without the large radiative correction [6–10]. This fact, along with the condition $\mu \lesssim 300$ GeV, makes the theory rather natural in predicting Z boson mass [11].

It should be noted that the lightest *CP*-even Higgs in the nNMSSM (denoted by h_1 hereafter) is rather peculiar. First, since it is lighter than about 120 GeV, its properties have been tightly limited by the large electron positron (LEP) experiments [12] and also by some analyses at the LHC [13,14]. Considering that the invariant mass of the diphoton signal can be determined rather precisely in an experiment, its future observation at colliders will provide a robust clue to popular singlet extensions of the SM, and it may also be used to distinguish the NMSSM from the MSSM, since the latter can not predict such a spectrum after considering relevant experimental constraints. Second, the recent dark matter (DM) direct detection experiments such as LUX and PandaX-II have imposed strong constraints on supersymmetric models [15]. In this case, the existence of a light *CP*-even Higgs boson is favored to relax the constraints since in certain parameter space, its contribution to the spin-independent (SI)

*junjiec@itp.ac.cn
†peiwen.wu123@gmail.com

cross section of DM-nucelon scattering is comparable but with an opposite sign to that of the SM-like Higgs boson so that the cross section is greatly reduced [15]. Finally, there are experimental hints on the existence of a light scalar. For example, both the LEP analysis on $Z\bar{b}b$ signal [16] and the recent compact muon solenoid (CMS) analysis on diphoton signal at LHC Run-I [14] have observed a 2σ excess over the corresponding background, which may be explained simultaneously by the presence of a CP-even Higgs boson with mass around 98 GeV (about NMSSM explanation of the $Zb\bar{b}$ excess, see [17–25]).

So far, there are numerous discussions on the properties of h_1 in nNMSSM and its future detection at the LHC [26–57], especially since the diphoton signal of h_1 at the LHC was intensively studied in [44–59]. These studies indicated that there exist some parameter regions where the couplings of h_1 with down-type quarks are more suppressed than those with up-type quarks and vector bosons so that the branching ratio of $h_1 \to \gamma\gamma$ can be greatly enhanced. In this case, the diphoton rate may be several times larger than its SM prediction for the same scalar mass [45]. In this work, we update previous studies in this subject by considering the constraints from DM physics, especially the impacts of the recent LUX and PandaX-II experiments [60–62] on the theory. Our results indicate that the DM experiments are very efficient in excluding the parameter space of nNMSSM, even if we assume that the lightest neutralino in the scenario constitutes only a small fraction of the DM in the Universe. As a result, previous results on the diphoton signal are exorbitantly optimistic. For example, compared with the latest study on the diphoton rate in [57], we find that the maximal theoretical prediction of the rate for $m_{h_1} = 80$ GeV drops from more than 120 fb to about 25 fb after including the constraints. We also consider the case of $m_{h_1} \simeq 98$ GeV to study whether nNMSSM can explain simultaneously the excesses reported by the LEP and CMS experiments. We conclude that even if the lightest neutralino is required to be solely responsible for the observed DM relic density, nNMSSM can still explain the excesses at 1σ level without violating any known constraint.

This paper is organized as follows. In Sec. II, we recapitulate the basics of the NMSSM, which are helpful to understand the results of this work. In Sec. III we investigate the diphoton rate of h_1 by performing an intensive scan over the vast parameter space of the NMSSM with various constraints. Different features of the rate are shown by deliberate figures. In Sec. IV we turn to investigate wether nNMSSM can simultaneously explain the excesses observed by the LEP and CMS experiments. Finally, we draw our conclusions in Sec. V.

II. BASICS OF THE NMSSM

As one of the most economical extensions of the MSSM, the NMSSM introduces one gauge singlet Higgs superfield in its matter content and usually adopts a Z_3 symmetry in the construction of its superpotential to avoid the appearance of dimensional parameters. In this work, we impose the Z_3 symmetry and the NMSSM superpotential and soft breaking terms in Higgs sector are [4]

$$W^{\rm NMSSM} = W_F + \lambda \hat{H}_u \cdot \hat{H}_d \hat{S} + \frac{1}{3}\kappa \hat{S}^3, \tag{1}$$

$$V_{\rm soft}^{\rm NMSSM} = \tilde{m}_u^2 |H_u|^2 + \tilde{m}_d^2 |H_d|^2 + \tilde{m}_s^2 |S|^2 + \left(\lambda A_\lambda S H_u \cdot H_d + \frac{1}{3}\kappa A_\kappa S^3 + \text{H.c.}\right), \tag{2}$$

where W_F is the superpotential of the MSSM without the μ-term and $\hat{H}_u$, $\hat{H}_d$ and $\hat{S}$ are Higgs superfields with H_u, H_d and S being their scalar components, respectively. The dimensionless coefficients of λ and κ parametrize the strengthes of the Higgs self couplings, and the dimensional quantities of $\tilde{m}_u$, $\tilde{m}_d$, $\tilde{m}_s$, A_λ, and A_κ are soft-breaking parameters. In practice, the squared masses of $\tilde{m}_u^2$, $\tilde{m}_d^2$, and $\tilde{m}_s^2$ are traded for m_Z, $\tan\beta \equiv v_u/v_d$, and $\mu \equiv \lambda v_s$ as theoretical inputs after considering the electroweak symmetry breaking conditions [4], where v_u, v_d, v_s represent the vacuum expectation value (vev) of H_u, H_d, S fields, respectively.

Due to the presence of the superfield $\hat{S}$, the NMSSM contains one more complex Higgs field S compared to the MSSM, and a singlino field that is the fermion component of $\hat{S}$. Consequently in the NMSSM there are three (two) CP-even (CP-odd) Higgs particles corresponding to the mixings of the real (imaginary) parts of the H_u, H_d, S fields, and five neutralinos composed of bino, wino, higgsino, and singlino fields. Throughout this paper, we denote these particles by h_i $(i = 1, 2, 3)$, A_i $(i = 1, 2)$ and $\tilde{\chi}_i^0$ $(i = 1, \cdots 5)$ respectively with the convention $m_{h_1} < m_{h_2} < m_{h_3}$, $m_{A_1} < m_{A_2}$ and $m_{\tilde{\chi}_1^0} < m_{\tilde{\chi}_2^0} < \cdots < m_{\tilde{\chi}_5^0}$. In the following, we briefly introduce the key features of these particles, which is helpful to understand the results of this work.

A. The Higgs sector

In order to present the mass matrices of the Higgs fields in a physical way, we rotate the fields H_u and H_d as [4]

$$H_1 = \cos\beta H_u + \varepsilon \sin\beta H_d^*, \qquad H_2 = \sin\beta H_u - \varepsilon \cos\beta H_d^*, \qquad H_3 = S, \tag{3}$$

where ε is an antisymmetric tensor with $\varepsilon_{12} = -\varepsilon_{21} = 1$ and $\varepsilon_{11} = \varepsilon_{22} = 0$. After this rotation, the redefined fields H_i $(i = 1, 2, 3)$ have the following form

$$H_1 = \begin{pmatrix} H^+ \\ \frac{S_1 + iP_1}{\sqrt{2}} \end{pmatrix}, \qquad H_2 = \begin{pmatrix} G^+ \\ v + \frac{S_2 + iG^0}{\sqrt{2}} \end{pmatrix}, \qquad H_3 = v_s + \frac{1}{\sqrt{2}}(S_3 + iP_2), \tag{4}$$

where H_2 corresponds to the SM Higgs doublet with G^+, G^0 being the Goldstone bosons eaten by W and Z bosons respectively, and H_1 represents a new $SU(2)_L$ doublet scalar field with no coupling to W and Z bosons at tree level.

In the CP-conserving NMSSM, the fields S_1, S_2, and S_3 mix to form three physical CP-even Higgs bosons. In the basis (S_1, S_2, S_3), the elements of the corresponding mass matrix are given by [4]

$$\begin{aligned}
M_{11}^2 &= M_A^2 + (m_Z^2 - \lambda^2 v^2)\sin^2 2\beta, \\
M_{12}^2 &= -\frac{1}{2}(m_Z^2 - \lambda^2 v^2)\sin 4\beta, \\
M_{13}^2 &= -\left(\frac{M_A^2}{2\mu/\sin 2\beta} + \kappa v_s\right)\lambda v \cos 2\beta, \\
M_{22}^2 &= m_Z^2 \cos^2 2\beta + \lambda^2 v^2 \sin^2 2\beta, \\
M_{23}^2 &= 2\lambda\mu v\left[1 - \left(\frac{M_A}{2\mu/\sin 2\beta}\right)^2 - \frac{\kappa}{2\lambda}\sin 2\beta\right], \\
M_{33}^2 &= \frac{1}{4}\lambda^2 v^2\left(\frac{M_A}{\mu/\sin 2\beta}\right)^2 + \kappa v_s A_\kappa \\
&\quad + 4(\kappa v_s)^2 - \frac{1}{2}\lambda\kappa v^2 \sin 2\beta,
\end{aligned} \tag{5}$$

where M_A represents the mass scale of the doublet field H_1, and is given by

$$M_A^2 \equiv m_{P_1 P_1}^2 = \frac{2\mu}{\sin 2\beta}(A_\lambda + \kappa v_s). \tag{6}$$

This mass matrix indicates that the squared mass of the SM Higgs field S_2, M_{22}^2, gets an additional contribution of $\lambda^2 v^2$ in comparison with the MSSM expression, and for $\lambda^2 v^2 > M_Z^2$, its tree-level value is maximized with $\tan\beta \simeq 1$. This matrix also indicates that if the relation $m_{S_3 S_3}^2 < m_{S_2 S_2}^2$ holds, the mixing between the fields S_2 and S_3 can further enhance the mass of the SM-like Higgs boson. In this case, h_1 is a singlet-dominate scalar while h_2 plays the role of the SM Higgs boson. Benefiting from the above contributions, $m_{h_2} \simeq 125$ GeV does not necessarily require a large radiative contribution from stop loops [6–10]. Due to this attractive feature, the scenario with h_2 corresponding to the SM-like Higgs boson was usually called natural NMSSM [5].

The mass matrix in Eq. (5) can be diagonalized by an orthogonal 3×3 matrix V, and consequently the physical states h_i are given by

$$h_i = \sum_{j=1}^{3} V_{ij} S_j. \tag{7}$$

With this notation, and also noting the fact that current LHC data have required the properties of the 125 GeV boson to highly mimic those of the SM Higgs boson, one can infer that the normalized couplings of h_1 in nNMSSM with SM particles take following form

$$\begin{aligned}
&C_{h_1 u\bar{u}} \simeq V_{11}\cot\beta + V_{12}, \\
&C_{h_1 d\bar{d}} \simeq V_{11}\tan\beta + V_{12}, \qquad C_{h_1 VV} = V_{12}.
\end{aligned} \tag{8}$$

Since sparticles and charged Higgs bosons are preferred to be heavy by the LHC so far, searches for new particles, their influence on the h_1 couplings is usually negligible [5]. Therefore we can approximate the diphoton rate of h_1 at the LHC by the following formula

$$\begin{aligned}
\sigma_{\gamma\gamma} &\equiv \sigma(gg \to h_1 \to \gamma\gamma) \\
&= \sigma(gg \to h_1) \times \mathrm{Br}(h_1 \to \gamma\gamma) \\
&\simeq C_{h_1 u\bar{u}}^2 \sigma_{\mathrm{SM}}(gg \to h_1)\frac{C_{h_1 u\bar{u}}^2 \Gamma_{\gamma\gamma}^{\mathrm{SM}}}{\Gamma_{\mathrm{tot}}} \\
&\simeq C_{h_1 u\bar{u}}^4 \frac{\Gamma_{\mathrm{tot}}^{\mathrm{SM}}}{\Gamma_{\mathrm{tot}}} \times \sigma_{\mathrm{SM}}(gg \to h_1)\mathrm{Br}_{\mathrm{SM}}(h_1 \to \gamma\gamma),
\end{aligned} \tag{9}$$

where σ_{SM} and $\mathrm{Br}_{\mathrm{SM}}$ are the cross section and branching ratio of a SM Higgs boson with same mass as h_1 respectively, and Γ_{tot} is the total width of h_1 given by

$$\begin{aligned}
\Gamma_{\mathrm{tot}} &= \Gamma_{b\bar{b}} + \Gamma_{c\bar{c}} + \Gamma_{\tau\bar{\tau}} + \Gamma_{gg} + \cdots \\
&\simeq C_{h_1 d\bar{d}}^2(\Gamma_{b\bar{b}}^{\mathrm{SM}} + \Gamma_{\tau\bar{\tau}}^{\mathrm{SM}}) + C_{h_1 u\bar{u}}^2(\Gamma_{c\bar{c}}^{\mathrm{SM}} + \Gamma_{gg}^{\mathrm{SM}}) + \cdots.
\end{aligned} \tag{10}$$

Equation (9) and Eq. (10) indicate that the diphoton rate of h_1 in nNMSSM may be moderately large if $C_{h_1 b\bar{b}} \simeq 0$ (achieved by accidental cancelation between $V_{11}\tan\beta$ and V_{12}), and meanwhile, $C_{h_1 u\bar{u}}$ is not suppressed too much. This is possible in some corners of the NMSSM parameter space [45,57], which is what we are interested in. These equations also imply that an enhanced diphoton rate is usually associated with a suppressed $b\bar{b}$ signal of h_1. This correlation can affect our explanation of the 98 GeV excesses observed by the LEP and CMS experiments. Throughout this work, we use the public code SusHi 1.5 [63] to obtain the next-to-next-to-leading order gluon fusion production cross section for a SM-like Higgs boson, and multiply it by the normalized ggh_1 coupling given by NMSSMTools [64] to get $\sigma(gg \to h_1)$. We checked that the cross section for the bottom fusion production of h_1 is usually significantly smaller than $\sigma(gg \to h_1)$, and thus can be safely neglected.

Similarly the fields P_1 and P_2 mix to form CP-odd Higgs bosons A_1 and A_2. One subtle point about the pseudoscalars is that the LHC search for nonstandard Higgs bosons has required the doublet-dominated one to be heavier than about 400 GeV, while the dominated one may still be arbitrarily light. An important application of this feature is that the mass of the singlet-dominated pseudoscalar can be

tuned around $2m_{\tilde{\chi}_1^0}$, so that a moderately light $\tilde{\chi}_1^0$ can annihilate it via the resonance to result in a correct relic density and also a sizable cross section for DM annihilation in the Galactic Center [65,66].

B. The neutralino sector

The neutralino sector of the NMSSM consists of the fields bino $\tilde{B}^0$, wino $\tilde{W}^0$, higgsinos $\tilde{H}_{d,u}^0$, and singlino $\tilde{S}^0$. Taking the basis of $\psi^0 = (-i\tilde{B}^0, -i\tilde{W}^0, \tilde{H}_d^0, \tilde{H}_u^0, \tilde{S}^0)$, one has the following symmetric neutralino mass matrix

$$\mathcal{M} = \begin{pmatrix} M_1 & 0 & -\frac{g_1 v_d}{\sqrt{2}} & \frac{g_1 v_u}{\sqrt{2}} & 0 \\ & M_2 & \frac{g_2 v_d}{\sqrt{2}} & -\frac{g_2 v_u}{\sqrt{2}} & 0 \\ & & 0 & -\mu & -\lambda v_u \\ & & & 0 & -\lambda v_d \\ & & & & \frac{2\kappa}{\lambda}\mu \end{pmatrix}, \quad (11)$$

where M_1 and M_2 are bino and wino soft breaking mass, respectively. With the rotation matrix N for the mass matrix, neutralino mass eigenstates are given by

$$\tilde{\chi}_i^0 = \sum_{j=1}^{5} N_{ij}\psi_j^0, \quad (12)$$

where the element N_{ij} parametrizes the component of the field ψ_j^0 in neutralino state $\tilde{\chi}_i^0$.

In supersymmetric models with R-parity conservation, the lightest neutralino $\tilde{\chi}_1^0$ acts as a promising DM candidate. Given that μ is usually smaller than about 300 GeV in nNMSSM [5,6] and the LHC searches for electroweakinos have required M_2 to be larger than about 350 GeV in simplified scenarios [67], one can infer that the dominant component of $\tilde{\chi}_1^0$ prefers to be any of the bino, singlino, and higgsinos. As has been pointed out by numerous studies, in this case $\tilde{\chi}_1^0$ may achieve an acceptable relic density in the following regions [15]

(i) The Higgs boson or Z boson resonance region, where the Higgs may be any of the three CP-even and two CP-odd Higgs bosons.
(ii) The coannihilation region, where $\tilde{\chi}_1^0$ is nearly degenerated with any of $\tilde{\chi}_1^{\pm}$, $\tilde{\chi}_2^0$ and $\tilde{l}$ ($\tilde{l}$ represents the lightest slepton).
(iii) The large mixing region, where $\tilde{\chi}_1^0$ has large higgsino and singlino fractions.

As for the DM physics in nNMSSM, two points should be noted. One is that since the higgsinos in nNMSSM are not heavy, i.e. $\mu \lesssim 300$ GeV, the higgsino components in $\tilde{\chi}_1^0$ are usually sizable, which can enhance the couplings of $\tilde{\chi}_1^0$ with Higgs and Z bosons. As a result, the cross sections of the DM-nucleon scattering tend to be large, and thus are subject to the constraints from DM direct detection experiments such as LUX and PandaX-II. In [15], we have shown that such constraints are very strong in excluding vast region in the $\lambda - \kappa$ plane, which implies that the parameter region where the diphoton signal of h_1 is optimal will inevitably be affected. In fact, this is one of our motivations to study the diphoton rate in light of the DM experiments. The other point is that in most viable case of nNMSSM, $\tilde{\chi}_1^0$ is singlino-dominated. Since the interactions of such a $\tilde{\chi}_1^0$ are rather weak, it usually annihilated in the early universe through the resonance of the singlet-dominated pseudoscalar to get an acceptable relic density. This also imposes nontrivial requirements on the parameter space of nNMSSM to affect the diphoton rate.

III. DIPHOTON RATE OF h_1 IN NNMSSM

In this section, we first perform a comprehensive scan over the parameter space of the Z_3 NMSSM by considering various experimental constraints, then we investigate the diphoton rate in its allowed parameter space. We present the features of the signal by deliberate figures.

A. Strategy in parameter scan

We begin our study by making some assumptions about unimportant supersymmetry (SUSY) parameters. These assumptions are consistent with current LHC search for sparticles, and they contain the following items:

(i) A gluino mass and all of the soft breaking parameters for the first two generation squarks are set to be 2 TeV.
(ii) All soft parameters in the third generation squark sector are treated as free parameters except that the relations $m_{U_3} = m_{D_3}$ for right-handed soft breaking masses and $A_t = A_b$ for soft breaking trilinear coefficients are assumed for the sake of simplicity.
(iii) All soft breaking parameters in the slepton sector take a common value $m_{\tilde{l}}$. This quantity mainly affects the muon anomalous magnetic moment.

With the above assumptions, we use the package NMSSMTools-5.0.1 [64] to scan the parameters of the Z_3 NMSSM as follows:

$$\begin{aligned} &0 < \lambda \leq 0.75, \quad 0 < \kappa \leq 0.75, \quad 2 \leq \tan\beta \leq 60, \\ &100\ \text{GeV} \leq m_{\tilde{l}} \leq 1\ \text{TeV}, \quad 100\ \text{GeV} \leq \mu \leq 1\ \text{TeV}, \\ &50\ \text{GeV} \leq M_A \leq 2\ \text{TeV}, \quad |A_\kappa| \leq 2\ \text{TeV}, \\ &100\ \text{GeV} \leq M_{Q_3}, \quad M_{U_3} \leq 2\ \text{TeV}, \\ &|A_t| \leq \min(3\sqrt{M_{Q_3}^2 + M_{U_3}^2}, 5\ \text{TeV}), \\ &20\ \text{GeV} \leq M_1 \leq 500\ \text{GeV}, \\ &100\ \text{GeV} \leq M_2 \leq 1\ \text{TeV}, \end{aligned} \quad (13)$$

where all of the parameters are defined at the scale of 2 TeV. To be more specific, we carry out two different sets of

Markov Chain scans to ensure that our results are as inclusive as possible. The first set of scans aim at getting the samples which satisfy the experimental upper bounds on DM relic density and DM-nucleon scattering cross sections, and the corresponding likelihood function we adopt is

$$\mathcal{L}=\mathcal{L}_{m_{h_2}}\times\mathcal{L}_{\mathrm{Br}(B\to X_s\gamma)}\times\mathcal{L}_{\mathrm{Br}(B_s\to\mu^+\mu^-)}\times\mathcal{L}_{\Omega h^2}\times\mathcal{L}_{\sigma_i}, \quad (14)$$

where $\mathcal{L}_{m_{h_2}}$, $\mathcal{L}_{\mathrm{Br}(B\to X_s\gamma)}$ and $\mathcal{L}_{\mathrm{Br}(B_s\to\mu^+\mu^-)}$ are likelihood functions for experimentally measured SM-like Higgs boson mass, $\mathrm{Br}(B\to X_s\gamma)$ and $\mathrm{Br}(B_s\to\mu^+\mu^-)$ respectively, which are taken to be Gaussian distributed, and $\mathcal{L}_{\Omega h^2}$ and $\mathcal{L}_{\sigma_i}$ denote the likelihood functions from the upper bounds on the DM observables with their explicit forms given in [68]. We select more than ten parameter points from the scan results in [15] which are well separated in $\lambda-\kappa$ plane as the starting points of the Markov Chain scans. This set of scans, as were shown by our practices, usually get samples with rather low h_1 diphoton rates. The second set of scans are designed to get the samples with a relatively large diphoton rate. For this end, we first scan the parameter space with the likelihood function

$$\mathcal{L}=\mathcal{L}_{m_{h_2}}\times\mathcal{L}_{\mathrm{Br}(B\to X_s\gamma)}\times\mathcal{L}_{\mathrm{Br}(B_s\to\mu^+\mu^-)}\times\mathcal{L}_{\sigma_{\gamma\gamma}},$$

where $\mathcal{L}_{\sigma_{\gamma\gamma}}=\exp\left[-(\sigma^{8\ \mathrm{TeV}}_{\mathrm{SM},\gamma\gamma}(h_1)/\sigma^{8\ \mathrm{TeV}}_{\gamma\gamma}(h_1))^2\right]$ is used to look for samples with large diphoton rates. After such a preliminary scan, we obtain some representative parameter points characterized by a large diphoton rate and meanwhile, moderately large DM observables. Taking them as starting points, we then scan the parameter space of the nNMSSM again, but this time the likelihood functions for the DM observables are included. Our results indicate that such a special treatment is essential to get the desired samples.

For the samples obtained in the scans, we further require them to explain at a 2σ level various B-physics observables, 125 GeV Higgs boson and muon anomalous magnetic moment, and satisfy the upper bounds set by LEP experiments, dark matter measurements, as well as ATLAS analysis on the diphoton signal of a light Higgs [13]. All of these quantities have been implemented in the package NMSSMTools-5.0.1. Moreover, we impose the constraints from the direct searches for Higgs bosons at Tevatron and LHC with the package HiggsBounds [69], the LHC searches for sparticles by detailed simulation,[1] and also the Fermi-LAT observation of a dwarf galaxy [70].

The constraints we consider here, differ from those of our previous works [11,15] in the following aspects.

(i) First, we allow for the possibility that $\tilde{\chi}_1^0$ constitutes a fraction of the DM observed in the Universe. In this case, the constraints from DM direct search experiments set an upper bound on the weighted DM-nucleon scattering cross section $\Omega_{\mathrm{LSP}}/\Omega_0\times\sigma_{\tilde{\chi}_1^0-n}$ with $\Omega_{\mathrm{LSP}}h^2$ and Ω_0h^2 denoting the relic density contributed by $\tilde{\chi}_1^0$ and the measured DM density from PLANK [71] and WMAP 9-year data [72] respectively. In practice, we use the latest bounds of the LUX and PandaX experiments on both spin-independent and spin-dependent (SD) scattering rates to set limits, and since a 10% theoretical uncertainty is usually assumed in calculating Ωh^2 by the package MicrOMEGAs [73], we consider $\tilde{\chi}_1^0$ as the sole DM candidate if $0.9\leq\Omega_{\mathrm{LSP}}/\Omega_0\leq 1.1$.

(ii) Second, we consider the constraint from the Fermi-LAT searches for DM-annihilation from dwarf galaxies. Since the DM annihilation for each parameter point usually includes a variety of channels in today's Universe, which is different from those single SM final states assumed by the Fermi-LAT collaboration to set bounds [70], we actually require the $\langle\sigma v\rangle$-weighted number of photon predicted by the parameter point to be less than that calculated with the Fermi-LAT bounds (see [74–76] for similar usage), i.e. $\langle\sigma v\rangle_{th}N_{\gamma,th}\lesssim\langle\sigma v\rangle_{\mathrm{exp}}N_{\gamma,\mathrm{exp}}$ where

$$N_{\gamma,th}=\int_{E_{\gamma,\min}}^{E_{\gamma,\max}}dE_\gamma\frac{dN_\gamma^{th}}{dE_\gamma},$$
$$N_{\gamma,exp}=\int_{E_{\gamma,\min}}^{E_{\gamma,\max}}dE_\gamma\frac{dN_\gamma^{\mathrm{exp}}}{dE_\gamma}, \quad (15)$$

with $\{E_{\gamma,\min},E_{\gamma,\max}\}=\{0.5,500\}$ GeV being the photon energy range analyzed in [70]. In more detail, we use the package MicrOMEGAs [73] to obtain the theoretical predictions $\langle\sigma v\rangle_{th}$ and

$$\frac{dN_\gamma^{th}}{dE_\gamma}=\sum_f Br^{(f)}\frac{dN_\gamma^{(f)}}{dE_\gamma}. \quad (16)$$

We choose $\langle\sigma v\rangle_{\mathrm{exp}}=\langle\sigma v\rangle_{b\bar{b}}$ which denotes the Fermi-LAT bound on the rate of the annihilation $\tilde{\chi}_1^0\tilde{\chi}_1^0\to b\bar{b}$ [70]. We also utilize the photon spectrum $dN_\gamma^{\mathrm{exp}}/dE_\gamma=dN_\gamma^{(b\bar{b})}/dE_\gamma$ generated by the code PPPC4DMID [77].

In order to check the validity of this simple way to implement the constraint, we alternatively use the method proposed in [78] and adopted in [79] to exclude parameter points. The latter method utilizes the likelihood function provided by the Fermi-LAT collaboration [80] and allows the variation of the J-factor for each dwarf galaxy. We find the two

[1] In our previous work [11], we introduced in detail how to implement the direct search constraints from LHC Run-I. Here we adopt the same way as [11] to impose the constraints.

methods are consistent as far as our samples are considered. A possible underlying reason for this is that for the excluded samples, DM annihilates mainly via the mediation of A_1 and consequently, the dominant final state is either $b\bar{b}$ or $t\bar{t}$. Since the shape of the spectrum $dN_\gamma^{(t\bar{t})}/dE_\gamma$ is similar to that of $dN_\gamma^{(b\bar{b})}/dE_\gamma$ for a given $m_{\tilde{\chi}_1^0}$, as a good approximation, one may simply scale the Fermi-LAT bound on $\langle\sigma v\rangle_{b\bar{b}}$ to get that for $\langle\sigma v\rangle_{t\bar{t}}$ [74–76]. Moreover, we also find that the Fermi-LAT constraint is rather weak and excludes only about 30 samples in our study. We checked that the excluded samples are featured by $100\ \text{GeV} < m_{\tilde{\chi}_1^0} < 200\ \text{GeV}$, $0.3 < N_{13}^2 + N_{14}^2 < 0.7$, $2m_{\tilde{\chi}_1^0} > m_{A_1}$ and $\langle\sigma v\rangle_{\text{Today}} \gtrsim 10^{-23}\ \text{cm}^3\ \text{s}^{-1}$. We remind that the condition $2m_{\tilde{\chi}_1^0} > m_{A_1}$ ensures that the DM annihilation rate is currently larger than that in the early Universe [65].

(iii) Third, we use the latest version of package NMSSMTools to calculate various observables. There are many improvements of this version over previous ones, especially with the help of the package Lilith [81] which utilizes the recently combined ATLAS and CMS analysis on 125 GeV Higgs at LHC Run-I [82] to limit the model.

(iv) Finally, in getting the physically viable samples of the nNMSSM, we do not require the fine tuning quantities Δ_h and Δ_Z to be less than an artificial value 50 as we did in [11,15], instead we only require that h_2 acts as the 125 GeV Higgs boson.

In the following discussion, only the samples satisfying all of the constraints mentioned above are considered. In Table I, we list the ranges of the dimensional parameters in Eq. (13) and their prediction on the mass spectrum of some particles. Note that these sparticle spectrums are compatible with the direct searches for SUSY at LHC Run-I.

B. Numerical results

Since most of the nNMSSM samples obtained in the scans have a small diphoton rate of h_1 and meanwhile span a much wide parameter space, considering all of them in the discussion will make the figures presented below rather disordered and obfuscate the main conclusions of this work. So, in this subsection we only consider those which predict $\sigma^{8\ \text{TeV}}_{\text{SUSY}}(pp \to h_1 \to \gamma\gamma)$, hereafter denoted as $\sigma^{8\ \text{TeV}}_{\gamma\gamma}$, larger than 15 fb to simplify our analysis.

TABLE I. Ranges of some dimensional parameters and masses in unit of GeV obtained in the scans of this work.

P_i	Range	Mass	Range	Mass	Range
M_1	66–350	$\tilde{t}_1$	670–1800	$\tilde{\chi}_1^0$	59–220
M_2	350–860	$\tilde{b}_1$	690–1850	$\tilde{\chi}_2^0$	70–280
M_A	485–1930	$\tilde{\tau}_1$	94–670	$\tilde{\chi}_1^\pm$	106–320
μ	104–330	A_1	28–420	$H_1^\pm$	470–1950

In the left panel of Fig. 1, we show $\sigma^{8\ \text{TeV}}_{\gamma\gamma}$ versus m_{h_1}, where the colors indicate how much $\tilde{\chi}_1^0$ constitutes the relic abundance today and the red dotted (blue solid) line corresponds to the current ATLAS (CMS) bounds on the rate. This figure shows that there are still plenty of nNMSSM samples that can evade current LHC searches for a light Higgs beyond the SM, despite that many of them can not solely account for the observed relic abundance. For these samples, the maximal prediction of the h_1 diphoton rate at 8 TeV LHC is significantly smaller than the prediction without considering the constraints from DM physics, which was presented in [57]. Taking m_{h_1} around 80 GeV as an example, we find that the signal rate can reach about 70 fb if one allows $\tilde{\chi}_1^0$ to constitute only a small fraction of the thermal relic (less than 10%), while it drops to about 25 fb when the full thermal relic is required. By contrast, the h_1 diphoton signal rate can exceed 120 fb if one completely ignores the DM restrictions, including both the thermal relic and the latest direct detection bounds [57]. Also, in some cases the DM constraints are stronger than the LHC bounds in limiting the diphoton signal, e.g. for $m_{h_1} \simeq 80$ GeV the ATLAS analysis requires $\sigma^{8\ \text{TeV}}_{\gamma\gamma} \lesssim 90$ fb, while the DM physics restrict $\sigma^{8\ \text{TeV}}_{\gamma\gamma} \leq 70$ fb.

We checked that the suppression of h_1 diphoton rate due to DM restrictions is generally over a wide range of h_1 mass, as can be seen from the sample distribution with a relatively large thermal relic (warm color) at the bottom of left panel of Fig. 1. To our best knowledge, this observation has not been emphasized sufficiently before and should receive reasonable attention if one considers the interplay between the Higgs (especially singlet extension) and the DM sector in supersymmetric models. Since our original intention is to exhibit this connection in a sense as general as possible by allowing a reasonably large number of NMSSM parameters to vary in the scan, a thoroughly analytical interpretation of the h_1 diphoton signal suppression related to DM constraints would be very difficult and nearly impossible. However, we can still get nontrivial hints based on two factors involved in the interplay. One is that $C_{h_1 b\bar{b}}$ coupling should be strongly suppressed in order to get an enhanced h_1 diphoton rate as indicated in Eqs. (9), (10), which limits the nNMSSM parameters to certain regions providing a proper cancellation suggested by Eq. (8), i.e.

$$V_{11}\tan\beta + V_{12} \sim 0, \tag{17}$$

where some detailed discussions about CP-even Higgs mass matrix determining rotation matrix V can found, e.g. in [51,83]. Another one comes from the direct detection constraints in which the coefficients of the scalar type effective DM-quark operator used in calculating SI DM-nucleon scattering rate should be suppressed, i.e.

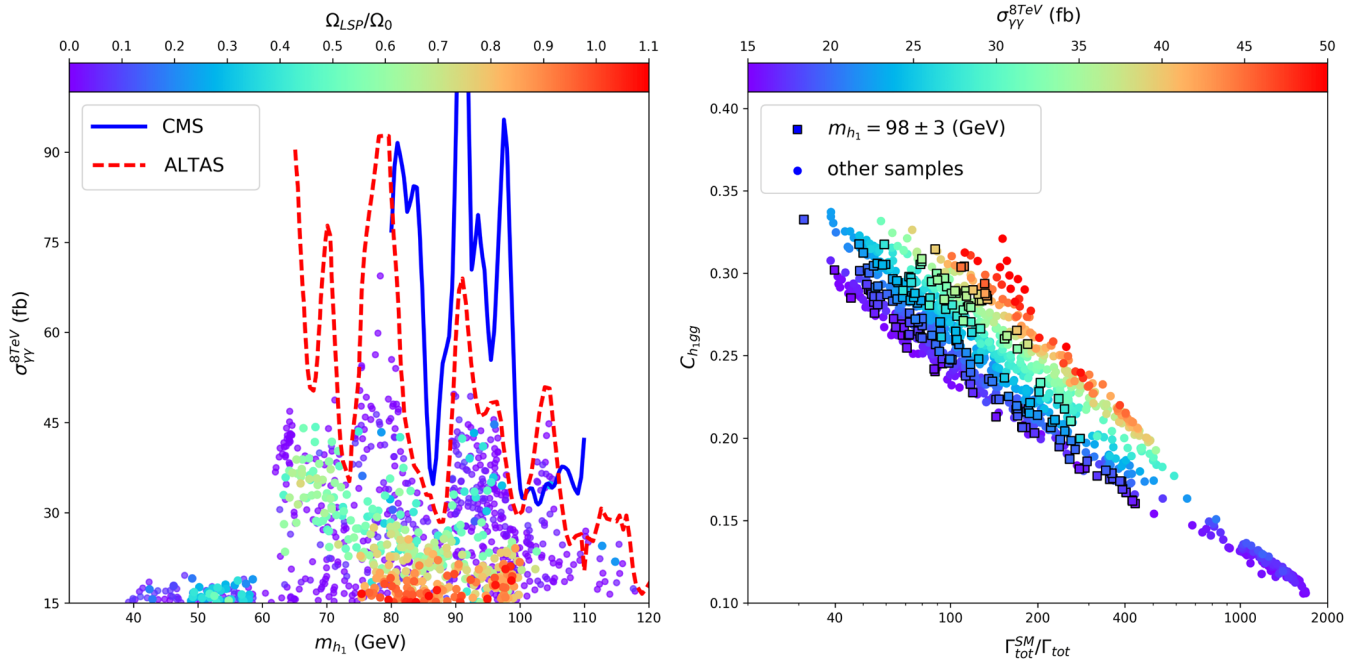

FIG. 1. *Left panel*: the diphoton rate of h_1 at 8 TeV LHC versus h_1 mass for the samples surviving the constraints in the scan and, meanwhile, predicting a moderate large diphoton rate, $\sigma_{\gamma\gamma}^{8\mathrm{TeV}} \geq 15$ fb. Colors in this panel indicate how much $\tilde{\chi}_1^0$ constitutes the relic abundance today and the red dotted (blue solid) line corresponds to the current ATLAS (CMS) bounds on the rate. *Right panel*: correlation of the normalized h_1-gluon-gluon coupling C_{h_1gg} to the ratio $\Gamma_{\mathrm{tot}}^{\mathrm{SM}}/\Gamma_{\mathrm{tot}}$ for the samples in the left panel with the colors indicating the magnitude of $\sigma_{\gamma\gamma}^{8\ \mathrm{TeV}}$. Γ_{tot} denotes the total width of h_1 predicted by the nNMSSM, and $\Gamma_{\mathrm{tot}}^{\mathrm{SM}}$ is the width of h_1 calculated by assuming that h_1 has same couplings as those of the SM Higgs boson. Squares in the panel represent samples with $m_{h_1} = 98 \pm 3$ GeV, which is the mass range favored by the LEP and CMS mild excesses.

$$\frac{C_{h_1\tilde{\chi}_1^0\tilde{\chi}_1^0} C_{h_1 NN}}{m_{h_1}^2} + \frac{C_{h_2\tilde{\chi}_1^0\tilde{\chi}_1^0} C_{h_2 NN}}{m_{h_2}^2} \sim 0, \tag{18}$$

where approximated formulae for $C_{h_i\tilde{\chi}_1^0\tilde{\chi}_1^0}$, $C_{h_i NN}$ can be found in [84,85] for DM scenarios featuring different dominant components. This requirement also puts strong constraints on the nNMSSM parameter space, especially those parameters shared in both two sectors such as $\{\lambda, \kappa, \tan\beta, \mu\}$. As a result, the Z_3 NMSSM compromises the two requirements and results in a moderately suppressed diphoton rate. Equation (18) actually corresponds to a well known scenario called Blind Spots (BS) in SUSY models like MSSM and NMSSM. We refer interested readers to [85–88] (and references therein) for more detailed discussions.

The left panel of Fig. 1 also shows that for an h_1 with mass smaller than $m_{h_2}/2 \approx 62$ GeV where the LHC diphoton bounds are not available, the diphoton signal are generally below 20 fb. This suppression is due to the kinematic opening of the exotic decay $h_2 \to h_1 h_1$ for the SM-like Higgs boson h_2, which receives strong constraints from the current Higgs measurement and thus pushes h_1 further to the singlet component corner. Another related case of $h_3 \to h_2 h_1$ in nNMSSM can be found in [89]. It should also be noted that in some other cases allowed by the DM constraints, the diphoton rates can be very close to the current LHC diphoton bounds. With the currently updated collision energy at 13 TeV LHC and the future high luminosity upgrade, these cases are very likely to be discovered or excluded.

In the right panel of Fig. 1 we show the normalized h_1-gluon-gluon coupling C_{h_1gg} to its SM prediction with the same Higgs mass versus the ratio of h_1 total width $\Gamma_{\mathrm{tot}}^{\mathrm{SM}}/\Gamma_{\mathrm{tot}}$ defined in Eq. (9). In this panel the colors indicate the magnitude of $\sigma_{\gamma\gamma}^{8\ \mathrm{TeV}}$ and the squares correspond to samples with $m_{h_1} = 98 \pm 3$ GeV, which is the mass range favored by the LEP and CMS diphoton mild excesses. One can learn that although the singlet-dominant nature of h_1 causes an overall suppression of its couplings to the SM fermions and thus to the gluons via the fermion loop, C_{h_1gg} can still reach about 0.35, which is crucial to obtain a sizable h_1 production cross section. On the other hand, a significant suppression of h_1 total width compared to its SM prediction[2] is also needed to increase the diphoton rate as indicated by Eq. (9). This is the natural consequence of the

[2]In the following when we use the phrase "its SM prediction," we mean the case where h_1 is identical to the Higgs boson in the SM except that its mass is adopted same as the prediction of the NMSSM.

dominant singlet component in h_1 that reduces the leading decay modes into $b\bar{b}$, $\tau^+\tau^-$. We checked that for the samples with $\sigma_{\gamma\gamma}^{8\,\mathrm{TeV}}$ around 30 fb, $\mathrm{Br}(h_1 \to b\bar{b})$ is usually below 30% compared to about 90% for its SM prediction, and $\mathrm{Br}(h_1 \to \gamma\gamma)$ can reach 3%.

As mentioned in Sec. I, the existence of a light h_1 is tightly limited not only from the LEP measurements but also from the DM observations. To pass the current stringent bounds from LUX and PandaX-II experiments, there must exist strong cancelations among the contributions of the three CP-even Higgs bosons, which would limit the nNMSSM parameter space into certain regions. In order to illustrate this expectation, in Fig. 2 we project the samples in Fig. 1 on $\tan\beta - \lambda$ planes (first row), $\kappa - \lambda$ planes (second row), $\mu - \lambda$ planes (third row), and $m_{H^\pm} - \lambda$ (last row) with the colors in left panels denoting the $\tilde{\chi}_1^0$ contribution to the thermal relic $\Omega_{\mathrm{LSP}}/\Omega_0$ and those in right panels representing the magnitude of $\sigma_{\gamma\gamma}^{8\,\mathrm{TeV}}$. Moreover, we also use dots, triangles, and squares in the left panels to denote samples with bino, higgsino, and singlino as the dominant component of $\tilde{\chi}_1^0$, respectively, and squares in the right panels to denote samples with $m_{h_1} = 98 \pm 3$ GeV. Obviously, given the horizontal axis assigned to singlet-doublet-doublet Higgs coupling coefficient λ for all panels, the samples only move vertically between panels with different paired nNMSSM parameters.

Figure 2 indicates that the samples in Fig. 1 are distributed in two isolated parameter regions, which are given by

(i) Region I: $0.1 \lesssim \lambda \lesssim 0.2$, $6 \lesssim \tan\beta \lesssim 20$, $0.02 \lesssim \kappa \lesssim 0.1$, $100\ \mathrm{GeV} \lesssim \mu \lesssim 190\ \mathrm{GeV}$, $1\ \mathrm{TeV} \lesssim m_{H^\pm} \lesssim 2\ \mathrm{TeV}$;

(ii) Region II: $0.45 \lesssim \lambda \lesssim 0.70$, $1.5 \lesssim \tan\beta \lesssim 3$, $0.1 \lesssim \kappa \lesssim 0.3$, $220\ \mathrm{GeV} \lesssim \mu \lesssim 330\ \mathrm{GeV}$, $450\ \mathrm{GeV} \lesssim m_{H^\pm} \lesssim 700\ \mathrm{GeV}$.

Since the colors in the left and right panels correspond to $\Omega_{\mathrm{LSP}}/\Omega_0$ and $\sigma_{\gamma\gamma}^{8\,\mathrm{TeV}}$ respectively, one can quickly identify that only part of samples in Region II can have $\tilde{\chi}_1^0$ capable of accounting for all of the DM relic density today.[3] For these samples, $\tilde{\chi}_1^0$ is singlino-dominated, which can be seen clearly from the enlarged region in the first row of Fig. 2. This can also be inferred from the relation of $2\kappa/\lambda < 1$ as shown in the second row of diagrams. We checked that $\tilde{\chi}_1^0$, for this case, annihilated in the early universe mainly through the s-channel exchange of a moderately light singlet-like A_1 to get an acceptable relic density.

As for Region II, one should note that the charged Higgs boson is moderately light and consequently, $\mathrm{Br}^{(th)}(B \to X_s\gamma)$ may deviate significantly from its SM prediction. We checked that the ratio varies from 3.75×10^{-4} to 4.2×10^{-4} (In NMSSMTools, the theoretical uncertainties are included in the calculation. So the central value of $\mathrm{Br}^{(th)}(B \to X_s\gamma)$ is allowed to vary in a broader range than its experimentally favored range). We also checked that in this region, $H^\pm$ is approximately degenerated in mass with H_3^0 and the doublet-dominated CP-odd Higgs boson. In our analysis, we have included the constraint on the neutral sector from the LHC direct searches for extra Higgs bosons in terms of $\tau\bar{\tau}$ final state [90] through both the package NMSSMTools and the package HiggsBounds.

To gain a sense of future detection potential of h_1 via the diphoton signal, in the left panel of Fig. 3 we show the diphoton rate $\sigma_{\gamma\gamma}^{14\,\mathrm{TeV}}$ versus m_{h_1}, which is similar to Fig. 1 but with $\sqrt{s} = 14$ TeV at the LHC. One can learn that a general cross section enhancement of 2–3 times can be achieved with the increased collision energy, e.g. for m_{h_1} around 80 GeV the diphoton signal rate can reach about 160 fb instead of 70 fb at 8 TeV LHC. On the right panel of Fig. 3 we further compare the h_1 diphoton rate to its SM prediction. We can see that despite the general suppression of the h_1 couplings to SM particles, an increased diphoton signal as large as 1.6 times can still be achievable in the light Higgs mass region due to the suppression of the h_1 total width. Note that the LHC as a hadron collider suffers from large hadronic background, and consequently, the diphoton signal is usually the most ideal channel to search for h_1 in spite of the fact that $b\bar{b}$ is generally the dominant decay mode of h_1. If the diphoton signal is discovered in future with a moderately large rate, Fig. 3 can provide us useful information about whether $\tilde{\chi}_1^0$ in the nNMSSM is capable of explaining all the DM density.

Since a future e^+e^- collider like Higgs factory TLEP [91,92] and circular electron positron collider [93] is very powerful in discovering possibly new light Higgs, we study the process $e^+e^- \to Zh_1$ followed by $h_1 \to b\bar{b}$, $\gamma\gamma$. In Fig. 4, we show the production rates of the two signals for the samples in Fig. 1. We present our results in term of the ratio of the rate to its SM prediction, which we would call normalized signal rate hereafter. Note that these normalized signal rates are independent of the collision energy. The left panel indicates that the $b\bar{b}$ signal rate of h_1 is usually strongly suppressed in comparison with its SM prediction, reaching at most 7% for the samples we considered. By contrast, the $\gamma\gamma$ signals have a signal ratio from mild suppression to an enhancement of 1.1 as indicated by the right panel. In order to estimate the

[3]We emphasize that only samples with $\sigma_{\gamma\gamma}^{8\,\mathrm{TeV}} \geq 15$ fb are shown in Fig. 2. If we do not consider such a requirement, the parameter λ for experimentally allowed samples will span a wide range from 0.03 to 0.7, and $\tilde{\chi}_1^0$ can account for the measured relic density at any value of λ [15]. We obtained this observation by intensive and time-consuming scans. During the process we also noticed that it was rather difficult to obtain nNMSSM samples satisfying all the constraints, especially when one requires $\tilde{\chi}_1^0$ to fully account for the relic density. This reflects the fact that parameters closely related to DM properties, such as λ, κ, $\tan\beta$, and μ, must collaborate properly to survive the constraints.

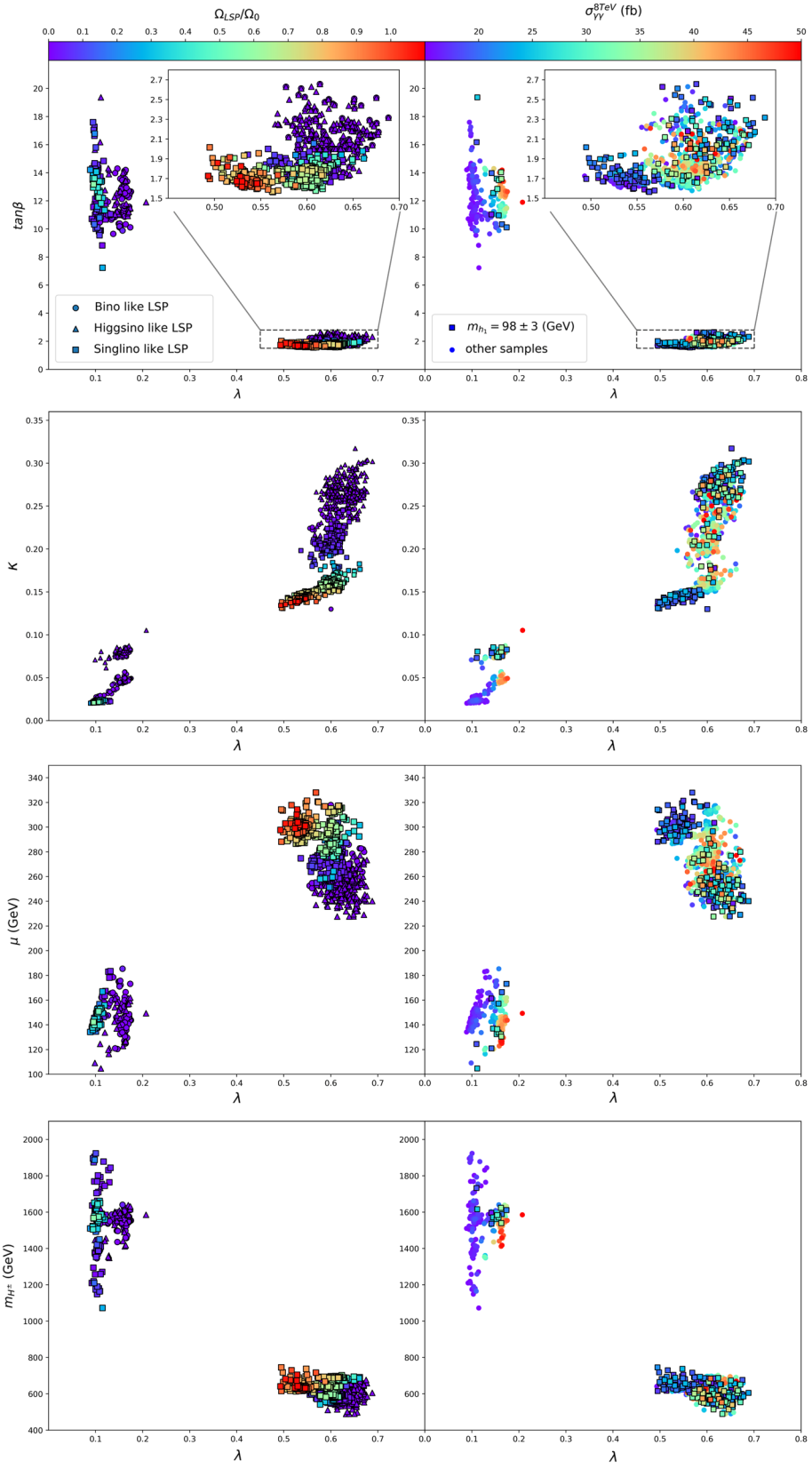

FIG. 2. Samples in Fig. 1 projected in different parameter planes. In the left panels, colors denote the $\tilde{\chi}_1^0$ contribution to the thermal relic $\Omega_{\rm LSP}/\Omega_0$, and dots, triangles, and squares represent samples with bino, higgsino, and singlino as the main component of $\tilde{\chi}_1^0$, respectively. In the right panels, colors represent the magnitude of $\sigma_{\gamma\gamma}^{8\ \rm TeV}$, and squares correspond to the samples with $m_{h_1} = 98 \pm 3$ GeV.

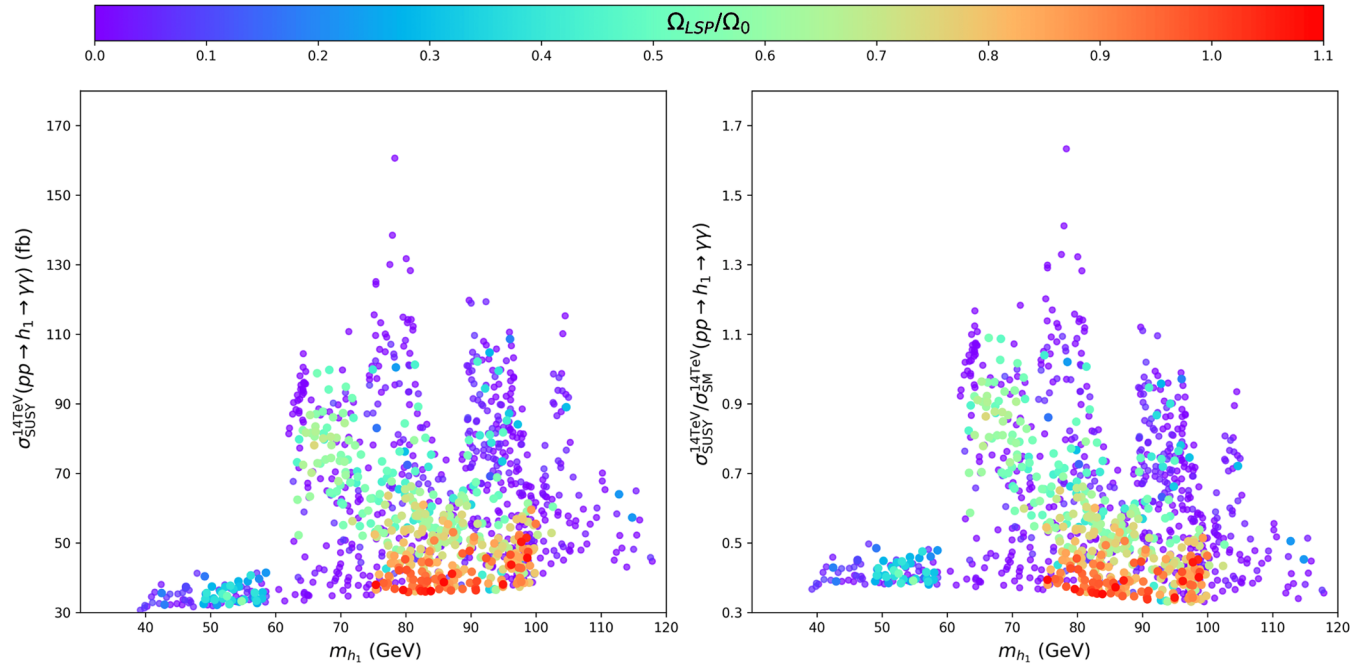

FIG. 3. Same as the left panel in Fig. 1, except that the vertical axes denote the diphoton rate at 14 TeV LHC. In the right panel, the ratio $\sigma^{14\text{ TeV}}_{\text{SUSY}}/\sigma^{14\text{ TeV}}_{\text{SM}}$ represents the normalized diphoton rate where the cross section $\sigma^{14\text{ TeV}}_{\text{SM}}(pp \to h_1 \to \gamma\gamma)$ is calculated by assuming that h_1 has the same couplings as those of the SM Higgs boson. Note that these normalized signal rates are independent of LHC collision energy in our case where the gluon fusion dominates the h_1 production.

sensitivity of the collider to the signals, we recall that the expected precision of determining the $b\bar{b}$ signal of the SM Higgs boson is around 0.1% for TLEP [94] (due to the large production rate of the signal as well as the clean background of the collider), and that for the diphoton signal is at a 3% level. So if we assume the sensitivities to detect h_1 signals to be at the same order as those of the 125 GeV Higgs boson, we can expect that most samples considered in this section have an opportunity of being explored by both the $b\bar{b}$ signal and the diphoton signal at TLEP.

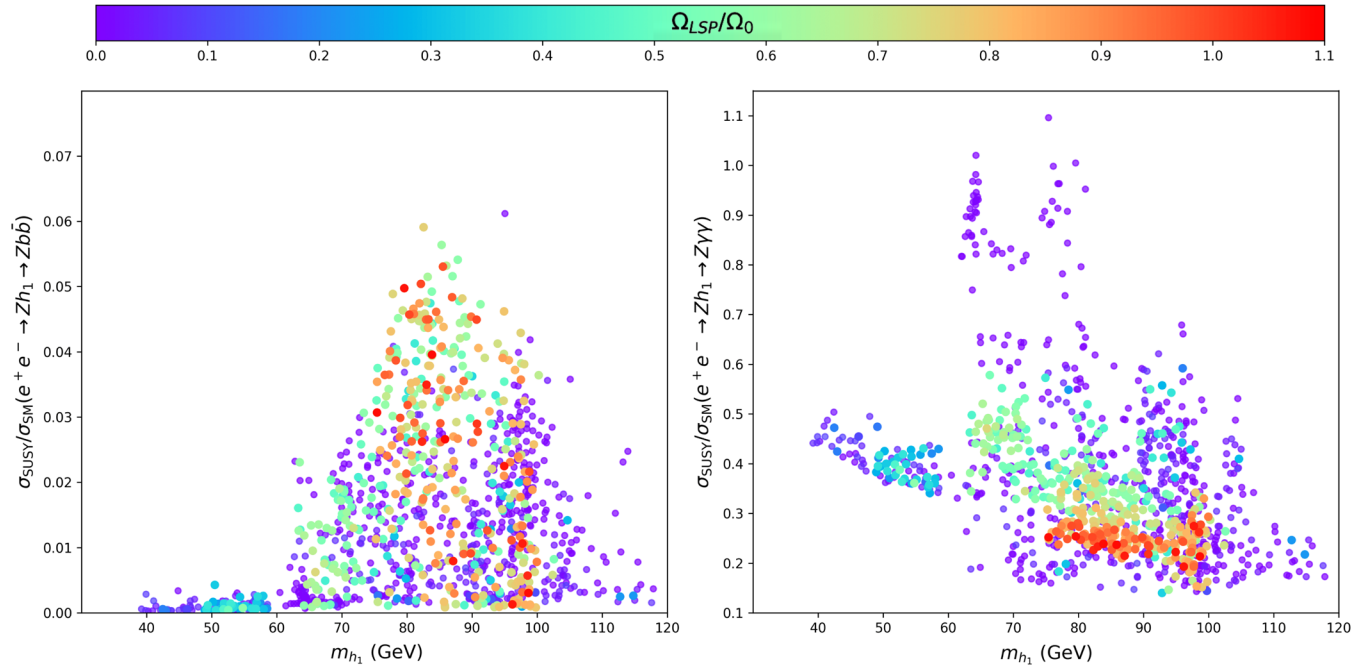

FIG. 4. Similar to the right panel of Fig. 3, but displaying the normalized rate for the process $e^+e^- \to Zh_1 \to Zb\bar{b}$ (left panel) and $e^+e^- \to Zh_1 \to Z\gamma\gamma$ (right panel). Note that these normalized rates are independent of e^+e^- collision energy.

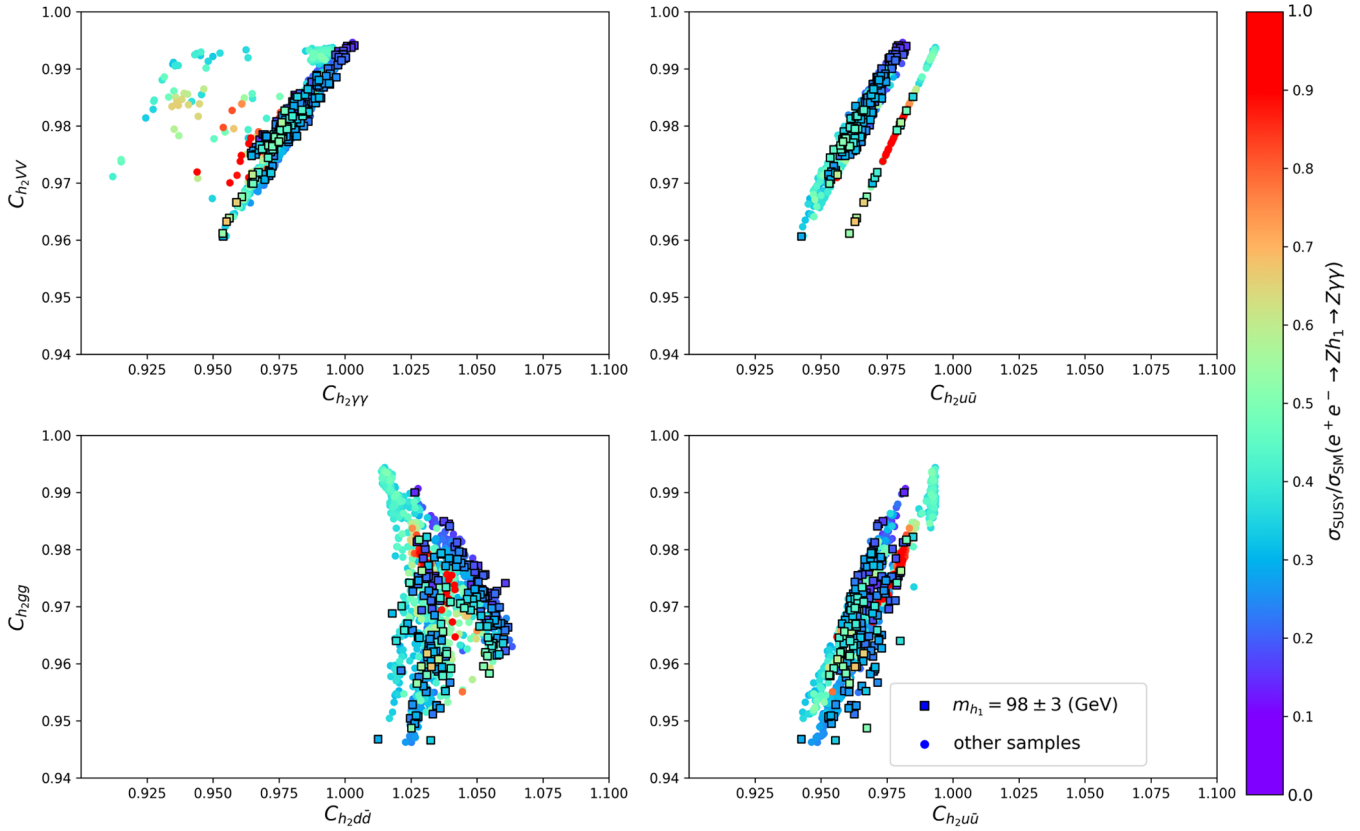

FIG. 5. Normalized couplings of the SM-like Higgs boson h_2 for the samples in Fig. 1 with colors denoting the normalized diphoton rate at future e^+e^- collider. This figure reflects the correlation of the h_2 couplings with the h_1 diphoton rate at e^+e^- collider.

Apart from the direct searches for h_1, one can also constrain the nNMSSM parameter space via its correlation with the properties of the SM-like Higgs boson which will be measured to a high precision at future e^+e^- collider (about 1.5% for $h_2\gamma\gamma$ coupling and 0.5% for the other couplings at TLEP [94]). In Fig. 5 we show various couplings of h_2 normalized to its SM value with the colors indicating the normalized rate for the process $e^+e^- \to Zh_1 \to Z\gamma\gamma$ to its SM prediction. Again, we use the squares to denote the samples with $m_{h_1} = 98 \pm 3$ GeV. From the figure it is obvious that if future Higgs precision measurement limits the normalized couplings within certain narrow regions, lots of currently available nNMSSM samples will be excluded and the properties of h_1 will be further limited. This fact implies that the precision measurement of the h_2 couplings plays a complementary role to the direct searches for the light Higgs h_1 at the e^+e^- collider. Moreover, since the two methods are independent, they can be used to crosscheck whether the NMSSM is the right underlying theory for the light Higgs boson once the existence of h_1 is confirmed in experiment.

Before we end this section, we have the following comments about our study:

(i) From our previous description, it is obvious that we actually repeated the work [57], where the constraints from DM physics on nNMSSM were neglected. We found that after including the constraints, more than 90% samples in our repetition were excluded and the allowed parameter region and the diphoton rate were affected significantly. We thank the authors of [57] for providing benchmark points in their work for comparison.

(ii) In order to crosscheck our results presented in this section, we also performed the same parameter scan by the package SARAH [95] which employs the code SPheno [96] as a spectrum generator. We found that we can reproduce the results obtained by NMSSMTools except that a longer time is needed in calculation.

(iii) The conclusion that the diphoton rate is strongly limited after considering the DM constraints may not be applied directly to other extensions of the Z_3 NMSSM. For example, in the general NMSSM model more free parameters enter the mass matrix for CP-even Higgs bosons and also that for neutralinos [4]. Consequently, the parameter space which predicts a suppressed $h_1 b\bar{b}$ coupling may still be compatible with DM observations and thus allow for an enhanced diphoton rate. Detailed analysis of this situation is beyond the scope of our work. Another example is the case in which Z_3 NMSSM is embedded in gauge mediated SUSY breaking framework (GMSB). In this scenario, a

light gravitino usually acts as a DM candidate (see [97,98] for reviews and [99] for recent attempts) and it can achieve correct relic density from a proper reheating history after inflation [100,101] and/or from next-to-lightest supersymmetric particle decays [102–105]. Meanwhile, due to its lightness and very weak couplings, the gravitino DM is easy to evade current and future direct detection bounds. Since the DM physics are quite different from that of the Z_3 NMSSM discussed in this work, its interplay with the diphoton rate should be very weak.

IV. EXPLANATION OF 98 GEV EXCESSES IN NNMSSM

In this section, we investigate whether nNMSSM can explain simultaneously the 98 GeV excesses observed by both LEP and CMS experiments. For this end, we first extract the favored signal rates from the 95% C.L. expected and observed exclusion limits in [14,16] with the method introduced in [106], which are

$$\hat{\mu}_{\rm LEP} = 0.117 \pm 0.057, \qquad \hat{\sigma}^{8\ \rm TeV}_{\gamma\gamma} = 41 \pm 25\ \text{fb}. \tag{19}$$

Then we build the following χ^2

$$\chi^2 = \frac{(\mu_{\rm LEP} - 0.117)^2}{0.057^2} + \frac{(\sigma^{8\ \rm TeV}_{\gamma\gamma} - 41)^2}{25^2} \tag{20}$$

to fit the excesses with the diphoton cross section $\sigma^{8\ \rm TeV}_{\gamma\gamma}$ in unit of fb. In Eq. (19), the first number on the right side of each formula denotes the central value of the corresponding h_1 signal, and the second number is the experimental uncertainty. The quantity $\mu_{\rm LEP}$ is defined by

$$\mu_{\rm LEP} = \frac{\sigma_{\rm NP}(e^+e^- \to Zh_1)}{\sigma_{\rm SM}(e^+e^- \to Zh_1)} \text{BR}(h_1 \to b\bar{b}), \tag{21}$$

where $\sigma_{\rm NP}(e^+e^- \to Zh_1)$ denotes new physics prediction on the cross section of the process $e^+e^- \to Zh_1$ at LEP-II.

In order to study the excesses in the framework of nNMSSM, we select some samples obtained in the scan with $m_{h_1} = 98 \pm 3$ GeV (here 3 GeV represents the theoretical uncertainty of m_{h_1}), and project them on $\sigma^{8\ \rm TeV}_{\gamma\gamma} - \mu_{\rm LEP}$ plane. The results are given in Fig. 6, where the colors indicate how much $\tilde{\chi}^0_1$ constitutes the relic abundance today. The horizontal and vertical blue dotted lines represent the central values of the two excesses respectively, and the dashed lines are their 1σ lower bounds. We also plot the boundary of the 1σ region favored by the excesses (blue solid line), which corresponds to $\chi^2 = 2.3$ for two degree of freedom. From the figure, one can learn that in the nNMSSM it is very difficult to produce the central values of the two excesses simultaneously, even though the central value of each excess can be reproduced separately and there exist lots of samples which can explain the excesses at 1σ level. We checked that two reasons can account for this conclusion. On the one hand, as we introduced in Section II, a large diphoton rate at the LHC needs a suppression of $\text{Br}(h_1 \to b\bar{b})$ and thus a suppressed $\mu_{\rm LEP}$. On the other hand, since the property of h_1 is correlated with that of the SM-like Higgs boson h_2, the constraints on the properties of h_2 from relevant LHC data forbid the associated existence of a large $\sigma^{8\rm TeV}_{\gamma\gamma}$ with a moderately large $\mu_{\rm LEP}$.

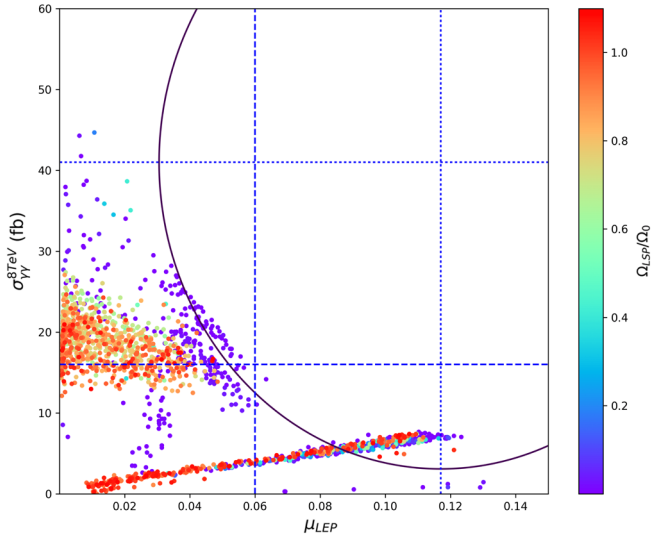

FIG. 6. nNMSSM explanation of the excesses observed by the LEP and CMS experiments where the colors denote the fraction of $\tilde{\chi}^0_1$ constituing the total DM. The horizontal and vertical blue dotted lines represent the central values of the two excesses respectively, and the dashed lines are their 1σ lower bounds. The boundary of the 1σ region for the excesses is also plotted as blue solid line.

Figure 6 also indicates that the samples with a low χ^2 can be classified into two categories by the value of $\sigma^{8\ \rm TeV}_{\gamma\gamma}$ and $\mu_{\rm LEP}$, which are

(i) Solution I: samples with $\sigma^{8\ \rm TeV}_{\gamma\gamma} \gtrsim 15$ fb and $\mu_{\rm LEP} \lesssim 0.06$ (see discussion in Section III);
(ii) Solution II: samples with $\sigma^{8\ \rm TeV}_{\gamma\gamma} \lesssim 10$ fb and $\mu_{\rm LEP} \gtrsim 0.06$.

In Table II, we list detailed information of four benchmark points for the excesses. Points P1 and P2 belong to Solution I and they predict $\chi^2 = 2.44$, $\Omega_{\rm LSP}/\Omega_0 \simeq 1$ and $\chi^2 = 2.05$, $\Omega_{\rm LSP}/\Omega_0 \ll 1$, respectively. For these two points, $V_{11}\tan\beta + V_{12}$ in Eq. (8) is more suppressed so that the normalized coupling $C_{h_1 b\bar{b}}$ is significantly smaller than the other couplings. However, a slight difference between the two points comes from the mass scale of the new Higgs doublet field m_A. Point P1 corresponds to a relatively small m_A, which usually implies a moderately large V_{11}. In this case a small $\tan\beta$ is needed for the cancelation between $V_{11}\tan\beta$ and V_{12}. On the contrary, point P2 predicts a large m_A and thus a small V_{11}, in which case a large $\tan\beta$ is necessary for the cancelation. Points P3 and P4 belong to Solution II and they have $\chi^2 = 1.78$, $\Omega_{\rm LSP}/\Omega_0 \simeq 1$ and $\chi^2 = 1.81$, $\Omega_{\rm LSP}/\Omega_0 \ll 1$, respectively. These two points are characterized by $V_{11} \simeq 0$ and as a result all normalized

TABLE II. Detailed information of four benchmark points for the 98 GeV excesses. These samples are take from Fig. 6 with the χ^2 as low as possible.

	$\mu_{\rm LEP}$	$\sigma_{\gamma\gamma}^{8\rm TeV}$	$\Omega_{\rm LSP}h^2$	λ	κ	$\tan\beta$	M_A	m_{h_1}	C_{h_1tt}	C_{h_1bb}	$C_{h_1\gamma\gamma}$	C_{h_1gg}	C_{h_1VV}
P1	0.042	19.9	0.112	0.566	0.142	1.8	714.6	96.4	0.092	0.017	0.106	0.099	0.069
P2	0.063	14.2	0.001	0.124	0.059	12.7	1641.1	98.1	0.092	0.029	0.110	0.098	0.092
P3	0.110	7.4	0.110	0.030	0.014	22.9	1638.4	100.1	0.136	0.120	0.140	0.138	0.136
P4	0.115	7.6	0.001	0.028	0.009	17.0	1615.9	99.7	0.141	0.128	0.147	0.144	0.141

couplings of h_1 are roughly equal. In this case, both the $b\bar{b}$ and $\gamma\gamma$ signal rate can be obtained from their SM predictions by multiplying the square of the common suppression factor for the couplings.

Finally, we emphasize that so far point P3 can explain the excesses in the best way, and at same time predicts the right relic density of DM. For this point, the $b\bar{b}$ signal rate is around the central value of the $Zb\bar{b}$ excess while the $\gamma\gamma$ rate is somewhat small and just around 7 fb. On the other hand, this point is at the edge of being excluded by current LHC data of the SM-like Higgs boson, which implies a potential tension of the LEP excess with the 125 GeV Higgs data.

V. CONCLUSION

As an attractive scenario, natural NMSSM (nNMSSM) can predict one CP-even Higgs boson satisfying $m_{h_1} \lesssim 120$ GeV and Higgsinos lighter than about 300 GeV. Consequently, the cross section for DM-nucleon scattering in this scenario is usually quite large, which implies that it will be tightly limited by the recent results of LUX and PandaX-II experiments. In this work, we first scan the parameter space of nNMSSM by considering various experimental constraints systematically. One main improvement of our study over previous ones is that we allowed the possibility of multiple DM candidates in the Universe by not requiring $\tilde{\chi}_1^0$ to be responsible for all of the measured DM relic density. We find that even with such a relaxed condition, the constraint from DM physics is still strong.

Next we considered the effect of DM physics on the diphoton rate of the light Higgs. We find that the optimal value of the signal rate at 8 TeV LHC is greatly reduced in comparison with earlier predictions. Taking m_{h_1} around 80 GeV as an example, the signal rate can reach about 70 fb if one allows $\tilde{\chi}_1^0$ to constitute only a small fraction of the thermal relic (less than 10%), and it drops to about 25 fb when the full thermal relic is required. By contrast, the h_1 diphoton signal rate can exceed 120 fb if one completely ignores the DM restrictions. We also briefly studied the detection potential of the light Higgs via the diphoton signal at future LHC and Higgs factory, and observed that they have a good chance of exploring some parameter space of the nNMSSM.

Finally, we investigated to what extent the nNMSSM can explain the 98 GeV excesses observed by both LEP and CMS experiments. We conclude that there exist lots of samples which can explain the excesses at 1σ level, even though the nNMSSM can not produce the central values of the two excesses simultaneously. The most favored samples of the nNMSSM predict the central value of the $Zb\bar{b}$ excess at LEP and a light Higgs diphoton rate at about 7 fb.

ACKNOWLEDGMENTS

We thank Prof. Ulrich Ellwanger and Dr. Matías Vázquez for helpful discussion about their works on diphoton rate, Prof. Guoming Chen for reminding us the diphoton excess observed by CMS collaboration, Prof. Xiaojun Bi, Yufeng Zhou, Pengfei Yin, and Weihong Zhang for their instructions about DM indirect searches, and Dr. Liangliang Shang for his help on Monte Carlo simulation of sparticle searches. This work is supported by the National Natural Science Foundation of China (NNSFC) under Grants No. 11575053 and No. 11275245.

[1] G. Aad *et al.* (ATLAS Collaboration), Phys. Lett. B **716**, 1 (2012).
[2] S. Chatrchyan *et al.* (CMS Collaboration), Phys. Lett. B **716**, 30 (2012).
[3] See for example, A. Arbey, M. Battaglia, A. Djouadi, F. Mahmoudi, and J. Quevillon, Phys. Lett. B **708**, 162 (2012).
[4] U. Ellwanger, C. Hugonie, and A. M. Teixeira, Phys. Rep. **496**, 1 (2010).
[5] S. F. King, M. Mhlleitner, R. Nevzorov, and K. Walz, Nucl. Phys. **B870**, 323 (2013).
[6] J. J. Cao, Z. X. Heng, J. M. Yang, Y. M. Zhang, and J. Y. Zhu, J. High Energy Phys. 03 (2012) 086.
[7] U. Ellwanger, J. High Energy Phys. 03 (2012) 044.

[8] Z. Kang, J. Li, and T. Li, J. High Energy Phys. 11 (2012) 024.
[9] S. F. King, M. Muhlleitner, and R. Nevzorov, Nucl. Phys. **B860**, 207 (2012).
[10] K. S. Jeong, Y. Shoji, and M. Yamaguchi, J. High Energy Phys. 09 (2012) 007.
[11] J. Cao, Y. He, L. Shang, W. Su, and Y. Zhang, J. High Energy Phys. 08 (2016) 037.
[12] See for example, K. S. Jeong, Y. Shoji, and M. Yamaguchi, J. High Energy Phys. 11 (2014) 148.
[13] G. Aad *et al.* (ATLAS Collaboration), Phys. Rev. Lett. **113**, 171801 (2014).
[14] CMS Collaboration, HIG-14-037
[15] J. Cao, Y. He, L. Shang, W. Su, P. Wu, and Y. Zhang, J. High Energy Phys. 10 (2016) 136.
[16] R. Barate *et al.* (LEP Working Group for Higgs boson searches and ALEPH and DELPHI and L3 and OPAL Collaborations), Phys. Lett. B **565**, 61 (2003).
[17] G. Belanger, U. Ellwanger, J. F. Gunion, Y. Jiang, S. Kraml, and J. H. Schwarz, J. High Energy Phys. 01 (2013) 069.
[18] L. Basso and F. Staub, Phys. Rev. D **87**, 015011 (2013).
[19] L. Aparicio, P. G. Camara, D. G. Cerdeno, L. E. Ibanez, and I. Valenzuela, J. High Energy Phys. 02 (2013) 084.
[20] D. G. Cerdeno, P. Ghosh, and C. B. Park, J. High Energy Phys. 06 (2013) 031.
[21] B. Bhattacherjee, M. Chakraborti, A. Chakraborty, U. Chattopadhyay, D. Das, and D. K. Ghosh, Phys. Rev. D **88**, 035011 (2013).
[22] K. Choi, S. H. Im, K. S. Jeong, and M. S. Seo, J. High Energy Phys. 01 (2014) 072.
[23] B. Allanach, M. Badziak, C. Hugonie, and R. Ziegler, *Proc. Sci.*, PLANCK2015 (2015) 012.
[24] B. Allanach, M. Badziak, C. Hugonie, and R. Ziegler, Phys. Rev. D **92**, 015006 (2015).
[25] M. Badziak and C. E. M. Wagner, J. High Energy Phys. 02 (2017) 050.
[26] A. Djouadi *et al.*, J. High Energy Phys. 07 (2008) 002.
[27] J. J. Cao, K. i. Hikasa, and W. Wang, Phys. Lett. B **703**, 292 (2011).
[28] M. Almarashi and S. Moretti, Phys. Rev. D **84**, 035009 (2011).
[29] O. Stal and G. Weiglein, J. High Energy Phys. 01 (2012) 071.
[30] A. Delgado, C. Kolda, and A. de la Puente, Phys. Lett. B **710**, 460 (2012).
[31] D. Das, U. Ellwanger, and A. M. Teixeira, J. High Energy Phys. 04 (2013) 117.
[32] N. D. Christensen, T. Han, Z. Liu, and S. Su, J. High Energy Phys. 08 (2013) 019.
[33] T. Cheng, J. Li, T. Li, and Q. S. Yan, Phys. Rev. D **89**, 015015 (2014).
[34] S. Moretti, S. Munir, and P. Poulose, Phys. Rev. D **89**, 015022 (2014).
[35] T. Cheng and T. Li, Phys. Rev. D **88**, 015031 (2013).
[36] J. Cao, F. Ding, C. Han, J. M. Yang, and J. Zhu, J. High Energy Phys. 11 (2013) 018.
[37] G. Cacciapaglia, A. Deandrea, G. Drieu La Rochelle, and J. B. Flament, Phys. Rev. D **91**, 015012 (2015).
[38] P. N. Pandita and M. Patra, Phys. Rev. D **89**, 115010 (2014).
[39] S. F. King, M. Mühlleitner, R. Nevzorov, and K. Walz, Phys. Rev. D **90**, 095014 (2014).
[40] F. Domingo and G. Weiglein, J. High Energy Phys. 04 (2016) 095.
[41] W. Wang, M. Zhang, and J. Zhao, arXiv:1604.00123.
[42] S. P. Das and M. Nowakowski, arXiv:1612.07241.
[43] M. Guchait and J. Kumar, Phys. Rev. D **95**, 035036 (2017).
[44] S. Moretti and S. Munir, Eur. Phys. J. C **47**, 791 (2006).
[45] U. Ellwanger, Phys. Lett. B **698**, 293 (2011).
[46] J. Cao, Z. Heng, T. Liu, and J. M. Yang, Phys. Lett. B **703**, 462 (2011).
[47] D. Albornoz Vasquez, G. Belanger, C. Boehm, J. Da Silva, P. Richardson, and C. Wymant, Phys. Rev. D **86**, 035023 (2012).
[48] U. Ellwanger and C. Hugonie, Adv. Ser. Dir. High Energy Phys. **2012**, 625389 (2012).
[49] F. Boudjema and G. D. La Rochelle, Phys. Rev. D **86**, 115007 (2012).
[50] K. Choi, S. H. Im, K. S. Jeong, and M. Yamaguchi, J. High Energy Phys. 02 (2013) 090.
[51] M. Badziak, M. Olechowski, and S. Pokorski, J. High Energy Phys. 06 (2013) 043.
[52] J. W. Fan, J.-Q. Tao, Y.-Q. Shen, G.-M. Chen, H.-S. Chen, S. Gascon-Shotkin, M. Lethuillier, L. Sgandurra, and P. Soulet, Chin. Phys. C **38**, 073101 (2014).
[53] M. Badziak, M. Olechowski, and S. Pokorski, *Proc. Sci.*, EPS-HEP2013 (2013) 257.
[54] M. Badziak, M. Olechowski, and S. Pokorski, arXiv:1406.1492.
[55] C. T. Potter, Eur. Phys. J. C **76**, 44 (2016).
[56] M. Guchait and J. Kumar, Int. J. Mod. Phys. A **31**, 1650069 (2016).
[57] U. Ellwanger and M. Rodriguez-Vazquez, J. High Energy Phys. 02 (2016) 096.
[58] K. Schmidt-Hoberg and F. Staub, J. High Energy Phys. 10 (2012) 195.
[59] R. Barbieri, D. Buttazzo, K. Kannike, F. Sala, and A. Tesi, Phys. Rev. D **88**, 055011 (2013).
[60] D. S. Akerib *et al.*, Phys. Rev. Lett. **118**, 021303 (2017).
[61] C. Fu *et al.* (PandaX-II Collaboration), Phys. Rev. Lett. **118**, 071301 (2017).
[62] A. Tan *et al.* (PandaX-II Collaboration), Phys. Rev. Lett. **117**, 121303 (2016).
[63] R. V. Harlander, S. Liebler, and H. Mantler, Comput. Phys. Commun. **184**, 1605 (2013).
[64] U. Ellwanger, J. F. Gunion, and C. Hugonie, J. High Energy Phys. 02 (2005) 066; U. Ellwanger and C. Hugonie, Comput. Phys. Commun. **175**, 290 (2006); G. Belanger, F. Boudjema, C. Hugonie, A. Pukhov, and A. Semenov, J. Cosmol. Astropart. Phys. 09 (2005) 001.
[65] J. Cao, L. Shang, P. Wu, J. M. Yang, and Y. Zhang, Phys. Rev. D **91**, 055005 (2015).
[66] See for example, J. Cao, L. Shang, P. Wu, J. M. Yang, and Y. Zhang, J. High Energy Phys. 10 (2015) 030.
[67] G. Aad *et al.* (ATLAS Collaboration), J. High Energy Phys. 04 (2014) 169.
[68] S. Matsumoto, S. Mukhopadhyay, and Y. L. S. Tsai, Phys. Rev. D **94**, 065034 (2016).

[69] P. Bechtle, O. Brein, S. Heinemeyer, G. Weiglein, and K. E. Williams, Comput. Phys. Commun. **181**, 138 (2010); P. Bechtle, O. Brein, S. Heinemeyer, G. Weiglein, and K. E. Williams, Comput. Phys. Commun. **182**, 2605 (2011).
[70] M. Ackermann *et al.* (Fermi-LAT Collaboration), Phys. Rev. Lett. **115**, 231301 (2015).
[71] P. A. R. Ade *et al.* (Planck Collaboration), Astron. Astrophys. **571**, A16 (2014).
[72] J. Dunkley *et al.* (WMAP Collaboration), Astrophys. J. Suppl. Ser. **180**, 306 (2009).
[73] G. Belanger, F. Boudjema, P. Brun, A. Pukhov, S. Rosier-Lees, P. Salati, and A. Semenov, Comput. Phys. Commun. **182**, 842 (2011).
[74] S. Baek, P. Ko, and P. Wu, J. High Energy Phys. 10 (2016) 117.
[75] T. Bringmann, X. Huang, A. Ibarra, S. Vogl, and C. Weniger, J. Cosmol. Astropart. Phys. 07 (2012) 054.
[76] F. Giacchino, A. Ibarra, L. Lopez Honorez, M. H. G. Tytgat, and S. Wild, J. Cosmol. Astropart. Phys. 02 (2016) 002.
[77] M. Cirelli, G. Corcella, A. Hektor, G. Hütsi, M. Kadastik, P. Panci, M. Raidal, F. Sala, and A. Strumia, J. Cosmol. Astropart. Phys. 03 (2011) 051; J. Cosmol. Astropart. Phys. 10 (2012) E01.
[78] L. M. Carpenter, R. Colburn, J. Goodman, and T. Linden, Phys. Rev. D **94**, 055027 (2016).
[79] X. J. Huang, C. C. Wei, Y. L. Wu, W. H. Zhang, and Y. F. Zhou, Phys. Rev. D **95**, 063021 (2017).
[80] see website: www-glast.stanford.edu/pub_data/1048.
[81] J. Bernon and B. Dumont, Eur. Phys. J. C **75**, 440 (2015).
[82] G. Aad *et al.* (ATLAS and CMS Collaborations), J. High Energy Phys. 08 (2016) 045.
[83] K. Agashe, Y. Cui, and R. Franceschini, J. High Energy Phys. 02 (2013) 031.
[84] M. Badziak, A. Delgado, M. Olechowski, S. Pokorski, and K. Sakurai, J. High Energy Phys. 11 (2015) 053.
[85] M. Badziak, M. Olechowski, and P. Szczerbiak, J. High Energy Phys. 03 (2016) 179.
[86] C. Cheung, L. J. Hall, D. Pinner, and J. T. Ruderman, J. High Energy Phys. 05 (2013) 100.
[87] P. Huang and C. E. M. Wagner, Phys. Rev. D **90** (2014) 015018.
[88] T. Han, F. Kling, S. Su, and Y. Wu, J. High Energy Phys. 02 (2017) 057.
[89] Z. Kang, J. Li, T. Li, D. Liu, and J. Shu, Phys. Rev. D **88**, 015006 (2013).
[90] CMS Collaboration, Report No. CMS-PAS-HIG-13-021.
[91] M. Koratzinos *et al.*, arXiv:1305.6498.
[92] M. Bicer *et al.* (TLEP Design Study Working Group Collaboration), J. High Energy Phys. 01 (2014) 164.
[93] See the website http://cepc.ihep.ac.cn/preCDR/volume.html.
[94] S. Dawson *et al.*, arXiv:1310.8361.
[95] F. Staub, Comput. Phys. Commun. **185**, 1773 (2014).
[96] W. Porod, Comput. Phys. Commun. **153**, 275 (2003).
[97] S. P. Martin, Adv. Ser. Dir. High Energy Phys. **21**, 1 (2010).
[98] C. F. Kolda, Nucl. Phys. B, Proc. Suppl. **62**, 266 (1998).
[99] K. Hamaguchi, M. Ibe, T. T. Yanagida, and N. Yokozaki, Phys. Rev. D **90**, 015027 (2014).
[100] L. M. Krauss, Nucl. Phys. **B227**, 556 (1983).
[101] D. V. Nanopoulos, K. A. Olive, and M. Srednicki, Phys. Lett. **127B**, 30 (1983).
[102] J. L. Feng, A. Rajaraman, and F. Takayama, Phys. Rev. Lett. **91**, 011302 (2003).
[103] J. L. Feng, A. Rajaraman, and F. Takayama, Phys. Rev. D **68**, 063504 (2003).
[104] J. R. Ellis, K. A. Olive, Y. Santoso, and V. C. Spanos, Phys. Lett. B **588**, 7 (2004).
[105] J. L. Feng, S. f. Su, and F. Takayama, Phys. Rev. D **70**, 063514 (2004).
[106] A. Azatov, R. Contino, and J. Galloway, J. High Energy Phys. 04 (2012) 127; J. High Energy Phys. 04 (2013) 140(E).